Fractionalization on the Surface: Is Type-II Terminated $1T$-TaS_2 Surface an Anomalously Realized Spin Liquid?

Chao-Kai Li,[1,2,*] Xu-Ping Yao,[1,2,*] Jianpeng Liu,[3,4] and Gang Chen[1,2,†]

[1]*Department of Physics and HKU-UCAS Joint Institute for Theoretical and Computational Physics at Hong Kong, The University of Hong Kong, Hong Kong, China*

[2]*The University of Hong Kong Shenzhen Institute of Research and Innovation, Shenzhen 518057, China*

[3]*School of Physical Science and Technology, ShanghaiTech University, Shanghai 200031, China*

[4]*ShanghaiTech Laboratory for Topological Physics, ShanghaiTech University, Shanghai 200031, China*

(Received 17 September 2021; revised 22 March 2022; accepted 8 June 2022; published 30 June 2022)

The type-II terminated $1T$-TaS_2 surface of a three-dimensional $1T$-TaS_2 bulk material realizes the effective spin-1/2 degree of freedom on each David star cluster with $\mathcal{T}^2 = -1$ such that the time-reversal symmetry is realized anomalously, despite the fact that bulk three-dimensional $1T$-TaS_2 material has an even number of electrons per unit cell with $\mathcal{T}^2 = +1$. This surface is effectively viewed as a spin-1/2 triangular lattice magnet, except with a fully gapped topological bulk. We further propose this surface termination realizes a spinon Fermi surface spin liquid with the surface fractionalization but with a nonexotic three-dimensional bulk. We analyze possible experimental consequences, especially the surface spectroscopic measurements, of the type-II terminated surface spin liquid.

DOI: 10.1103/PhysRevLett.129.017202

There has been great interest in the theoretical community to classify distinct topological phases with or without symmetry [1–10]. These include classifying different symmetric spin liquids and classifying symmetry-enriched topological orders and symmetry protected topological phases. Questions like where to realize the classified topological states were raised and partially understood [8]. It was understood that two-dimensional (2D) spin liquids (and/or 2D intrinsic topological orders) with certain symmetry fractionalizations cannot be realized in strictly 2D systems [8,11]. Instead, they may be realized on the 2D surface of the three-dimensional (3D) symmetry protected topological states where the symmetry is realized anomalously [8]. Likewise, similar results were established in the study of time-reversal symmetric 3D U(1) spin liquids where time-reversal symmetry is realized anomalously for the spinons and supports gapless surface liquid states [7,12]. Despite the interesting theoretical advances, such anomalous realizations of the low-dimensional spin liquids on the surface of the high-dimensional topological states, including those that can in principle be realized in strictly low-dimensional systems, have not yet been achieved.

In this Letter, we turn to the material's side and point out that the 3D multilayer-stacked $1T$-TaS_2 can be a candidate to anomalously realize the 2D spin liquid on its surface. This system has several interesting properties that differ from the conventional magnets. With the 3D multilayer stacking, the system develops the dimerization between neighboring layers along the z direction such that there exist even number of layers in each unit cell (see Fig. 1). The system develops a $\sqrt{13} \times \sqrt{13}$ charge-density-wave order at low temperatures, and the TaS_2 layer distorts to form cluster units with the shape of the Star of David. There exist 13 electrons in each Star of David, and thus one unpaired electron in the cluster unit. As the 3D system has even TaS_2 layers in the unit cell, the whole system is connected to a band insulator with a band gap, and we do not expect exotic quantum phases to emerge in the bulk. This is actually compatible with the Lieb-Schultz-Mattis-Oshikawa-Hastings (LSMOH) theorem that states the possibility of topological order and spin liquids in insulators with odd electron fillings [13–15]. The surface of this material, however, makes a difference. Because of the dimerization, there exist two distinct surface terminations [16] (see Fig. 1). The type-I (type-II) surface terminates at the end (middle) of the dimer. In this Letter, we provide a theoretical understanding of two different surfaces and argue that the type-II surface is an anomalously realized spin liquid.

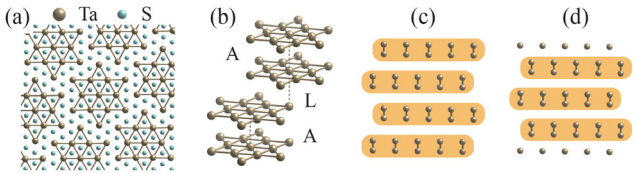

FIG. 1. (a) The Star of David clusters. After the charge-density-wave transition, the Ta—Ta bonds are contracted, forming a $\sqrt{13} \times \sqrt{13}$ supercell structure. (b) The out-of-plane stacking structure. The A-type and the L-type stacking occur alternately, which is referred to as the AL stacking. (c) Schematic of the type-I termination. (d) Schematic of the type-II termination.

The observation is to consider the 1D chain built from the coupling of the Star of David cluster along the z direction. Once one turns on the electron hopping along the chain, the model becomes a spinful version of the Su-Schrieffer-Heeger (SSH) model [17] if one neglects the displacement of the dimers from the neighboring layers. As shown in Figs. 1(c) and 1(d), the van der Waals bonds between the neighboring layers in the same dimer (in orange) are relatively strong, while those between different dimers are weak. The 1D chain supports gapless end states if the system terminates at the middle of the strong bond just like the type-II surface termination. Because of the spin part, the end states form a Kramers doublet with $\mathcal{T}^2 = -1$. As each David star hosts one unpaired electron, in the real space picture, two electrons from the strong bond pair up, leaving the electron on the end of the chain unpaired. When the 3D system is formed as in Fig. 1(d), the bulk is a band insulator while the surface is a 2D metal with an electron Fermi surface in our band structure calculation without including the strong correlation effect. When the electron correlation is included, the charge of the surface electron is clusterly localized in the David star, and the surface becomes Mott insulating. The remaining spin-1/2 degrees of freedom form a spin liquid. This surface spin-1/2 moment is anomalously realized, and so is the surface spin liquid. If the top surface of the system is type I and the bottom surface is type II, this "thick" 2D system would have an odd electron filling, and the presence of surface spin liquid is compatible with the LSMOH theorem.

The electronic structures of 1T-TaS_2 are calculated by a first-principles method within the Kohn-Sham scheme of density functional theory (DFT) [18,19], as implemented in the Quantum ESPRESSO package [20,21]. Details can be found in the Supplemental Material (SM) [22]. We use the AL stacking structure [see Fig. 1(b)], which was found to have the lowest energy previously [31–33]. This stacking sequence leads to dimerization along the z direction. The resulting Ta—Ta bond lengths in the star varies from 3.17 Å to 3.28 Å. The interlayer distance is around 6.7 Å, which is larger than the experimental value 5.92 Å [34]. Adding the van der Waals force corrections can get a smaller interlayer distance, but does not qualitatively change the surface states shown below due to the topological nature of the SSH model. Following the convention in the literature [31,32], the bulk band structure is plotted along the high-symmetry lines in the Brillouin zone of the $1 \times 1 \times 1$ primitive cell [22], as shown in Fig. 2(a). As a result of the dimerization, the bulk band of the dimerized TaS_2 is gapped. To obtain the low-energy model, we select the conduction and the valence band around the Fermi level, and construct the maximally localized Wannier functions using the WANNIER90 package [35,36]. The band structure of the resulting two-band tight-binding (TB) model is plotted by red crosses in Fig. 2(a). It can be seen that the TB band structure well reproduces the DFT result.

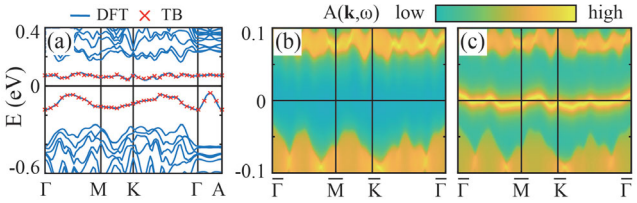

FIG. 2. (a) The band structure of bulk 1T-TaS_2 along the high-symmetry lines in the Brillouin zone of the primitive cell. The DFT and the tight-binding model results are shown by blue curves and red crosses, respectively. The spectral functions $A(\boldsymbol{k}, \omega)$ of the type-I and type-II terminated semi-infinite models are shown in (b) and (c), respectively.

To investigate the surface states of different terminations, we calculate the Green's function of the semi-infinite model based on the bulk two-band TB model, utilizing an iterative procedure [37] implemented in the WannierTools program [38]. The corresponding spectral functions for the type-I and type-II terminations are shown in Figs. 2(b) and 2(c), respectively. It is clearly seen that the type-I surface is gapped. In contrast, for the type-II termination, although the bulk is a band insulator, there is a surface band locating in the bulk gap. We have verified that the states on the surface band are indeed located on the surface (see the SM [22]). This surface band is half filled, making the type-II surface a two-dimensional metal if we neglect the correlation effects.

What would be the fate of this surface metal once the strong electron correlation is included? A large Kondo resonance was recently detected on the type-II surface upon the Pb doping [39], indicating the presence of the surface local moments. Moreover, early works on the monolayer 1T-TaS_2 indicate a cluster Mott insulating state where the unpaired electron from each Star of David is Mott localized and forms the local spin-1/2 moment [40–47]. Based on these results, we propose, upon introducing the electron correlation, the surface electron is localized via Mott transition [22] and forms the spin-1/2 Kramers doublet in each Star of David with $\mathcal{T}^2 = -1$. This anomalously realized spin-1/2 moment on the surface rises from the combination of the type-II surface and the Mott localization. Effectively, the surface becomes a spin-1/2 triangular lattice magnet, and this triangular lattice is the superlattice formed by the clusters. Like the situation for 1T-TaS_2 monolayer [40,42], we expect that the type-II surface realizes a spinon Fermi surface spin liquid.

This anomalously realized spin liquid, once formed on the type-II 1T-TaS_2 surface, could be detected indirectly by the angle-resolved photoemission. Here we propose an indirect spectroscopic detection scheme based on the surface coverage by a metallic layer. This differs from the direct spectroscopic measurement of the Mott insulating surface spin liquid [48]. We consider a conducting layer with itinerant electrons dosed on top of the type-II 1T-TaS_2

surface. A similar setup has been experimentally realized with graphene to investigate the proximity effect through scanning tunneling microscopy and spectroscopy quite recently [49]. The conducting layer contains itinerant electrons that interact with the underlying unpaired electrons of the $1T$-TaS_2 surface as

$$H_e = -\frac{t_e}{2}\sum_{\langle ij\rangle\sigma}(c^\dagger_{i\sigma}c_{j\sigma} + \text{H.c.}) - \mu_e\sum_{i\sigma}c^\dagger_{i\sigma}c_{i\sigma} + \sum_{\langle ik\rangle\sigma\sigma'}K_{ik}(c^\dagger_{i\sigma}\boldsymbol{\tau}_{\sigma\sigma'}c_{i\sigma'})\cdot\mathbf{S}_k, \quad (1)$$

where $c^\dagger_{i\sigma}$ ($c_{i\sigma}$) creates (annihilates) an electron with spin σ at site i on the conducting layer, t_e is the hopping parameter, μ_e is the chemical potential, and $\boldsymbol{\tau}$ are the Pauli matrices. $\mathbf{S}$ is the spin degree of freedom of the unpaired electrons on the cluster that is coupled to itinerant electrons via the Kondo-Hund coupling parameter K. Here the Kondo-Hund coupling is treated as a probing coupling for the emergent surface spinons. For the surface spin liquid of $1T$-TaS_2, the electron experiences a spin-charge separation where the charge sector is Mott localized while the spin sector is in the spin liquid phase. Without loss of generality, we consider a mean-field theory to incorporate the surface spinons that are described by a mean-field Hamiltonian,

$$H_s = -\sum_{\langle ij\rangle\sigma}t_{s,ij}(f^\dagger_{i\sigma}f_{j\sigma} + \text{H.c.}) - \mu_s\sum_{i\sigma}f^\dagger_{i\sigma}f_{i\sigma}, \quad (2)$$

where $t_{s,ij}$ refers to the spinon hopping on the triangular lattice formed by the cluster, and $f^\dagger_{i\sigma}$ and $f_{i\sigma}$ (with $\mathbf{S}_i = f^\dagger_{i\sigma}[\boldsymbol{\sigma}_{\sigma\sigma'}/2]f_{i\sigma'}$) are the spinon creation and annihilation operators on the cluster of the surface triangular superlattice. The chemical potential μ_s enforces the half filling constraint. For the uniform spinon hoppings with $t_{s,ij} = t_s/2$, the mean-field theory describes the spinon Fermi surface U(1) spin liquid.

The coupling to the conduction electrons could significantly modify the effective removal operator of electrons in the Mott insulator and thus result in the energy gains of the photoelectric effect. Physically, the ejected electrons carry the information from both the conduction and the Mott insulating layers. In the weak Kondo-Hund coupling limit, it has been shown that, in addition to the pure electron part, there exists an intertwined spin and charge response at the leading order due to the convolution of the itinerant electron spectral function $A_e(\boldsymbol{k},\omega)$ with the spin correlation function $\mathcal{S}(\boldsymbol{k},\omega)$ of the Mott insulating layer [50],

$$A(\boldsymbol{k},\omega\le 0) \propto \int_{-\infty}^{0}\frac{d\omega'}{2\pi}\int\frac{d^2\boldsymbol{q}}{(2\pi)^2}K(\boldsymbol{q}) \times A_e(\boldsymbol{q},\omega')\mathcal{S}(\boldsymbol{k}-\boldsymbol{q},\omega-\omega'), \quad (3)$$

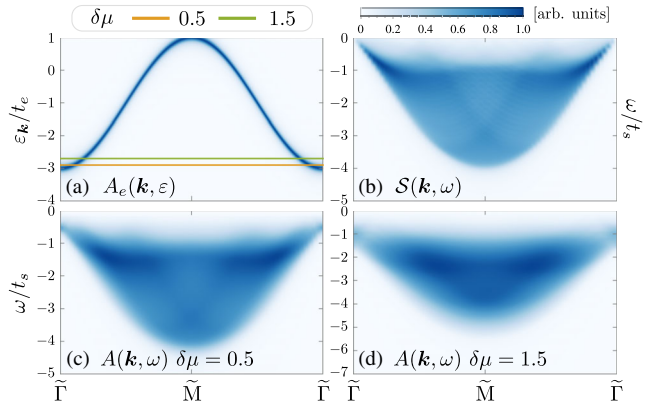

FIG. 3. (a) The spectral function $A_e(\boldsymbol{k},\varepsilon)$ for conduction electrons. Colored lines refer to Fermi levels for two dilute fillings where differences between the chemical potential μ_e and the band minimum $\varepsilon_{\min}$ take $\delta\mu = 0.5$ and 1.5, respectively. (b) The spin correlation $\mathcal{S}(\boldsymbol{k},\omega)$ of U(1) spin liquid with the spinon Fermi surface. (c),(d) The intertwined electron spectral function $A(\boldsymbol{k},\omega)$ for dilute fillings shown in (b). The electron hopping is fixed to $t_e = 5t_s$.

where $K(\boldsymbol{q})$ describes the Kondo-Hund coupling between the itinerant electrons and the spins, and the spin correlation function $\mathcal{S}(\boldsymbol{q},\omega) = \int_{-\infty}^{\infty}dt e^{i\omega t}\langle\mathbf{S}_{-\boldsymbol{q}}\cdot\mathbf{S}_{\boldsymbol{q}}(t)\rangle$. Note that $\mathcal{S}(\boldsymbol{q},\omega)$ vanishes for $\omega > 0$ [22]. When the Mott insulating layer is a spin ordered state, the spin correlation $\mathcal{S}(\boldsymbol{q},\omega)$ diverges at the ordering wave vector $\mathbf{Q}$ and the zero frequency $\omega = 0$, resulting in $A(\boldsymbol{k},\omega<0) \propto K(\boldsymbol{k}-\mathbf{Q})A_e(\boldsymbol{k}-\mathbf{Q},\omega)$. It can be immediately inferred that the intertwined spectral function manifests as a replica of itinerant electron bands but is shifted by the wave vector $-\mathbf{Q}$ and modulated by the Kondo-Hund coupling in intensity.

The intertwined signal for the spin liquid state is, however, quite different from the replica scenario because the spin correlation is a continuum both in momenta and frequency. The discrepancy stems from the peculiar energy distribution of the photoelectric effect in Eq. (3). The spectral function for conduction electrons can be approximated by $A_e(\boldsymbol{q},\omega') \approx \delta(\omega'-\xi_{\boldsymbol{q}})$, in which $\xi_{\boldsymbol{q}}$ is the difference between the electron energy $\varepsilon_{\boldsymbol{q}}$ and the chemical potential μ_e. Equation (3) can be reduced to

$$A(\boldsymbol{k},\omega\le 0) \propto \int_{\omega\le\xi_{\boldsymbol{q}}\le 0}\frac{d^2\boldsymbol{q}}{(2\pi)^2}K(\boldsymbol{q})\mathcal{S}(\boldsymbol{k}-\boldsymbol{q},\omega-\xi_{\boldsymbol{q}}). \quad (4)$$

For the integration domain, we have used the fact that both $A_e(\boldsymbol{q},\omega)$ and $\mathcal{S}(\boldsymbol{q},\omega)$ are restricted in the nonpositive frequency range $\omega\le 0$. Experimentally, the energy $\xi_{\boldsymbol{q}}$ can be shifted by tuning the electron chemical potential μ_e via gating. In the dilute limit, only a small number of electrons lie in the Fermi pocket around $\boldsymbol{q} = \tilde{\Gamma}$. Within this pocket, $\xi_{\boldsymbol{q}}$ can be approximated by $-\delta\mu + \boldsymbol{q}^2/2m^*$, where $\delta\mu = \mu_e - \varepsilon_{\min}$ is the difference between the chemical

potential μ_e and the band minimum $\varepsilon_{\min}$, and m^* is the effective mass of electron. Moreover, the intensity modulation from the momentum-dependent Kondo-Hund coupling $K(\boldsymbol{q})$ can be treated as a constant $K(\widetilde{\Gamma})$ in this approximation. For the case $-\delta\mu > \omega$, the domain of integration in Eq. (4) can be replaced by $-\delta\mu \leq \xi_{\boldsymbol{q}} \leq 0$ and the leading order term turns out to be

$$A(\boldsymbol{k}, \omega \leq 0) \propto \mathcal{S}(\boldsymbol{k}, \omega + \delta\mu)\delta\mu. \tag{5}$$

On the other hand, for small ω such that $-\delta\mu < \omega$, we have $A(\boldsymbol{k}, \omega \leq 0) \propto \mathcal{S}(\boldsymbol{k}, \omega + \delta\mu)\delta\omega = 0$ because now the frequency argument of $\mathcal{S}$ is positive. In any case, the information from the dynamic spin structure of the surface spin liquid can be conveyed into the intertwined spectral function as Eq. (5).

To quantitatively demonstrate the intertwined resonance, we calculate the spectral weights for a metallic layer on top of the surface spin liquid based on the complete convolution Eq. (3) directly. For numerical convenience, the metallic layer is set to match the triangular spin superlattice of $1T$-TaS_2 and they are AA stacked so that the final results are uniformly modulated by the Kondo-Hund coupling $K(\boldsymbol{q})$. As argued previously, such a uniform modulation is always expected in the dilute limit. More complicated coupling modulations corresponding to distinct stackings can be simulated and compared to the experimental results similarly. Given that the spinon band width is much smaller than that of the conduction electrons, we take t_s as the energy unit and set $t_e = 5t_s$ hereafter. The numerical results for different electron fillings are presented in Figs. 3 and 4 for high-symmetry momenta and a fixed frequency, respectively. The evolution of $A(\boldsymbol{k}, \omega)$ for more general fillings can be found in the SM [22].

In Fig. 3(a), we present the spectral function $A_e(\boldsymbol{k}, \varepsilon)$ for noninteracting electrons in the conducting layer. Two Fermi levels corresponding to dilute fillings with $\delta\mu = 0.5$ and 1.5 are indicated by colored lines. Figure 3(b) shows the spin correlation $\mathcal{S}(\boldsymbol{k}, \omega)$ of the U(1) spin liquid described by the free-spinon Hamiltonian Eq. (2). Because of the presence of the spinon Fermi surface, the particle-hole excitation can occur until the limit with zero energy transfer. At finite frequencies, the allowed momentum transfer excitations encode the spinon band information into the intensity of the spin correlation. This rich structure can be well captured by the intertwined electron spectral function $A(\boldsymbol{k}, \omega)$ at the dilute limit as shown in Fig. 3(c) where $\delta\mu = 0.5$. The slight broadening of fine structures comparing to Fig. 3(b) can be attributed to the scattering between spinons and the electrons with finite energy and momentum. Away from the dilute limit, these scatterings become more pronounced and the detailed features of the spin correlation are inevitably blurred, as shown in Fig. 3(d). There is an overall shift of the intertwined spectral function in frequency when tuning the electron filling. The displacement is at the order of $\delta\mu$ as predicted by the theoretical analysis.

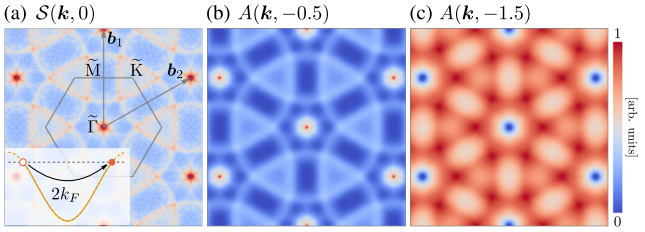

FIG. 4. (a) The momentum dependence of the spin correlation $\mathcal{S}(\boldsymbol{k}, 0)$. The inset shows the spinon excitation with zero energy transfer, which is the origin of the enhanced intensities near the circles with radius $2k_F$. Constant-energy images of the intertwined electron spectral function $A(\boldsymbol{k}, \omega)$ are calculated with (b) $(\delta\mu, \omega) = (0.5, -0.5)$ and (c) $(\delta\mu, \omega) = (1.5, -1.5)$.

Near the zero frequency, the spinon Fermi surface further supports particle-hole excitations with the $2k_F$ momentum transfer as sketched in the inset of Fig. 4(a). As a consequence of such type of excitations, the momentum distribution of $\mathcal{S}(\boldsymbol{k}, 0)$ features pronounced overlapping circles with radius $2k_F$ [see Fig. 4(a)]. The $2k_F$ feature has also been predicted in the static spin structure factor and treated as the necessary condition for detecting spin liquids with the spinon Fermi surface [42]. Our simulations reveal that this feature can be clearly reconstructed in the intertwined spectral function $A(\boldsymbol{k}, \omega)$ after the convolution in the dilute limit, as shown in Fig. 4(b) where $\delta\mu = 0.5$. Considering the overall shift [compare Figs. 3(b) and 3(a)], we have taken the frequency $\omega = -\delta\mu = -0.5$. Again, with the increase of the electron filling, the $2k_F$ circles become blurry, but are still discernible, as shown in Fig. 4(c) for $\omega = -\delta\mu = -1.5$.

The above results suggest that the angle-resolved photoemission spectroscopy (ARPES) could measure the spin correlation function in principle. In real measurements, the spectrum of a pure conduction layer and a pure surface state, which can be measured separately, should be treated as the background signal of the combined system and subtracted. What remains is the convolution of the itinerant electron's spectral function and the spin correlation function. These signals may have been detected but hide in the ARPES data of $1T$-$TaSe_2$ and $1T$-TaS_2 [45,51]. Furthermore, raw ARPES spectra are a convolution between the electron spectral function and the momentum and energy resolution of the experiment. Deconvolution procedures are usually used to mitigate noises from the instruments [52,53]. Interestingly, the itinerant electron's spectral function in Eq. (3) serves as a known resolution function instead. Similar deconvolution methods might be applied here to decode the spin correlation even with general fillings, once the intrinsic and intertwined electron spectral functions are obtained properly.

Discussion.—We discuss other experimental consequences of the surface spin liquid. The surface gapless

modes give an extra contribution to the low-temperature heat capacity in this bulk-gapped material. It means that the powderlike samples would have a higher heat capacity than the single-crystal samples. As the large Kondo resonance has already been observed in Pb-doped type-II terminated surface [39], this suggests the local moment formation and Mott physics, and further local probes such as nuclear magnetic resonance, should be helpful to detect the spin fluctuation on this surface. Thermal conductivity measurement can be a useful diagnosis of the gapless charge-neutral surface mode. There will be a magnetic contribution to thermal conductivity from type-II surface, while there is no magnetic thermal conductivity in type-I surface. The comparison between these two surface thermal transports can be quite insightful. The caveat is that the pure magnetic contribution may be difficult to obtain and may mix with the phonon transport. Since the monolayer $1T$-TaS_2 is believed to be proximate to the Mott transition [42], it is then reasonable to expect the type-II surface to be in the weak Mott regime and the thermal Hall transport result to apply [54]. Moreover, by varying the substrates to tune the surface electron correlations, it is likely to access the surface Mott transition and explore the universal transport properties associated with the (continuous) transition between the metal and surface spin liquid [22,23] directly.

The boundary terminated *exotic* liquid states are quite rare in condensed matter systems. Most were conventional states such as the Dirac-cone surface state for topological insulator and Luttinger liquids for quantum Hall effects [55–57]. For magnetic systems, the 2D spin-1 compound FeSe was suggested to form a coupled Haldane chain whose edge state would be a gapless spin-$1/2$ Heisenberg chain [58] and is well understood. A possible exotic state may emerge on the 2D surface of the spin-1 pyrochlore antiferromagnet, $Tl_2Ru_2O_7$, that was previously suggested as a possible formation of Haldane chains in 3D [59]. This would strongly depend on the orientation of Haldane chains, the surface lattice, and the interacting model for the emergent spin-$1/2$ degrees of freedom on the surface. There can be a triangular lattice or a kagome lattice on the (111) surface. In this regard, the type-II surface of $1T$-TaS_2 might be the first anomalous realization of exotic quantum liquid phase. Finally, in addition to the surface termination, the fault surface inside the bulk $1T$-TaS_2 could behave much like the type-II termination and could further support such an anomalous spin liquid.

To summarize, we explain the emergence of the spin-$1/2$ triangular lattice magnet on the type-II surface of the $1T$-TaS_2 and point out the possible existence of the spin liquid state. This spin liquid is anomalously realized and the experimental signatures are discussed.

We thank Shichao Yan, Yuan Li, and Chenjie Wang for useful discussions, and Patrick Lee and Vic Law for previous collaboration. The first-principles calculations for this work were performed on Tianhe-2 supercomputer. We are thankful for the support from the National Supercomputing Center in Guangzhou (NSCC-GZ). This work is supported by the National Science Foundation of China with Grant No. 92065203, the Ministry of Science and Technology of China with Grants No. 2018YFE0103200 and No. 2021YFA1400300, the Shanghai Municipal Science and Technology Major Project with Grant No. 2019SHZDZX01, and the Research Grants Council of Hong Kong with General Research Fund Grant No. 17306520.

*These authors contributed equally to this work.
†gangchen@hku.hk

[1] Z.-C. Gu and X.-G. Wen, Tensor-entanglement-filtering renormalization approach and symmetry-protected topological order, Phys. Rev. B **80**, 155131 (2009).
[2] X.-G. Wen, Classifying gauge anomalies through symmetry-protected trivial orders and classifying gravitational anomalies through topological orders, Phys. Rev. D **88**, 045013 (2013).
[3] X. Chen, Z.-C. Gu, Z.-X. Liu, and X.-G. Wen, Symmetry protected topological orders and the group cohomology of their symmetry group, Phys. Rev. B **87**, 155114 (2013).
[4] X. Chen, Z.-X. Liu, and X.-G. Wen, Two-dimensional symmetry-protected topological orders and their protected gapless edge excitations, Phys. Rev. B **84**, 235141 (2011).
[5] A. Vishwanath and T. Senthil, Physics of Three-Dimensional Bosonic Topological Insulators: Surface-Deconfined Criticality and Quantized Magnetoelectric Effect, Phys. Rev. X **3**, 011016 (2013).
[6] X. Chen, Z.-C. Gu, and X.-G. Wen, Classification of gapped symmetric phases in one-dimensional spin systems, Phys. Rev. B **83**, 035107 (2011).
[7] C. Wang and T. Senthil, Time-Reversal Symmetric $U(1)$ Quantum Spin Liquids, Phys. Rev. X **6**, 011034 (2016).
[8] A. M. Essin and M. Hermele, Classifying fractionalization: Symmetry classification of gapped $\mathbb{Z}_2$ spin liquids in two dimensions, Phys. Rev. B **87**, 104406 (2013).
[9] Z. Bi, A. Rasmussen, K. Slagle, and C. Xu, Classification and description of bosonic symmetry protected topological phases with semiclassical nonlinear sigma models, Phys. Rev. B **91**, 134404 (2015).
[10] A. Mesaros and Y. Ran, Classification of symmetry enriched topological phases with exactly solvable models, Phys. Rev. B **87**, 155115 (2013).
[11] H. Song and M. Hermele, Space-group symmetry fractionalization in a family of exactly solvable models with $\mathbb{Z}_2$ topological order, Phys. Rev. B **91**, 014405 (2015).
[12] D. Pesin and L. Balents, Mott physics and band topology in materials with strong spin–orbit interaction, Nat. Phys. **6**, 376 (2010).
[13] M. Oshikawa, Topological Approach to Luttinger's Theorem and the Fermi Surface of a Kondo Lattice, Phys. Rev. Lett. **84**, 3370 (2000).
[14] M. B. Hastings, Lieb-Schultz-Mattis in higher dimensions, Phys. Rev. B **69**, 104431 (2004).
[15] E. Lieb, T. Schultz, and D. Mattis, Two soluble models of an antiferromagnetic chain, Ann. Phys. (N.Y.) **16**, 407 (1961).

[16] C. J. Butler, M. Yoshida, T. Hanaguri, and Y. Iwasa, Mottness versus unit-cell doubling as the driver of the insulating state in 1T-TaS_2, Nat. Commun. **11**, 2477 (2020).

[17] A. J. Heeger, S. Kivelson, J. R. Schrieffer, and W. P. Su, Solitons in conducting polymers, Rev. Mod. Phys. **60**, 781 (1988).

[18] P. Hohenberg and W. Kohn, Inhomogeneous electron gas, Phys. Rev. **136**, B864 (1964).

[19] W. Kohn and L. J. Sham, Self-consistent equations including exchange and correlation effects, Phys. Rev. **140**, A1133 (1965).

[20] P. Giannozzi *et al.*, Quantum ESPRESSO: A modular and open-source software project for quantum simulations of materials, J. Phys. Condens. Matter **21**, 395502 (2009).

[21] P. Giannozzi *et al.*, Advanced capabilities for materials modelling with Quantum ESPRESSO, J. Phys. Condens. Matter **29**, 465901 (2017).

[22] See Supplemental Material at http://link.aps.org/supplemental/10.1103/PhysRevLett.129.017202 for detailed information, which includes Refs. [16,23–30].

[23] T. Senthil, Theory of a continuous Mott transition in two dimensions, Phys. Rev. B **78**, 045109 (2008).

[24] J. P. Perdew, K. Burke, and M. Ernzerhof, Generalized Gradient Approximation Made Simple, Phys. Rev. Lett. **77**, 3865 (1996).

[25] M.-C. Cha, M. P. A. Fisher, S. M. Girvin, M. Wallin, and A. P. Young, Universal conductivity of two-dimensional films at the superconductor-insulator transition, Phys. Rev. B **44**, 6883 (1991).

[26] W. Witczak-Krempa, P. Ghaemi, T. Senthil, and Y. B. Kim, Universal transport near a quantum critical Mott transition in two dimensions, Phys. Rev. B **86**, 245102 (2012).

[27] L. Zhang and F. Wang, Unconventional Surface Critical Behavior Induced by a Quantum Phase Transition from the Two-Dimensional Affleck-Kennedy-Lieb-Tasaki Phase to a Néel-Ordered Phase, Phys. Rev. Lett. **118**, 087201 (2017).

[28] A. Dal Corso, Pseudopotentials periodic table: From H to Pu, Comput. Mater. Sci. **95**, 337 (2014).

[29] https://dalcorso.github.io/pslibrary/.

[30] V. Sunko, F. Mazzola, S. Kitamura, S. Khim, P. Kushwaha, O. J. Clark, M. D. Watson, I. Markovi, D. Biswas, L. Pourovskii, T. K. Kim, T.-L. Lee, P. K. Thakur, H. Rosner, A. Georges, R. Moessner, T. Oka, A. P. Mackenzie, and P. D. C. King, Probing spin correlations using angle-resolved photoemission in a coupled metallic/Mott insulator system, Sci. Adv. **6**, eaaz0611 (2020).

[31] T. Ritschel, H. Berger, and J. Geck, Stacking-driven gap formation in layered 1T-TaS_2, Phys. Rev. B **98**, 195134 (2018).

[32] S.-H. Lee, J. S. Goh, and D. Cho, Origin of the Insulating Phase and First-Order Metal-Insulator Transition in 1T-TaS_2, Phys. Rev. Lett. **122**, 106404 (2019).

[33] W. Wang, C. Si, W. Lei, F. Xiao, Y. Liu, C. Autieri, and X. Ming, Stacking order and Coulomb correlation effect in the layered charge density wave phase of 1T-NbS_2, Phys. Rev. B **105**, 035119 (2022).

[34] F. Givens and G. Fredericks, Thermal expansion of $NbSe_2$ and TaS_2, J. Phys. Chem. Solids **38**, 1363 (1977).

[35] N. Marzari and D. Vanderbilt, Maximally localized generalized Wannier functions for composite energy bands, Phys. Rev. B **56**, 12847 (1997).

[36] G. Pizzi *et al.*, Wannier90 as a community code: New features and applications, J. Phys. Condens. Matter **32**, 165902 (2020).

[37] M. P. L. Sancho, J. M. L. Sancho, J. M. L. Sancho, and J. Rubio, Highly convergent schemes for the calculation of bulk and surface Green functions, J. Phys. F **15**, 851 (1985).

[38] Q. Wu, S. Zhang, H.-F. Song, M. Troyer, and A. A. Soluyanov, WannierTools: An open-source software package for novel topological materials, Comput. Phys. Commun. **224**, 405 (2018).

[39] S. Shen, C. Wen, P. Kong, J. Gao, X. Luo, W. Lu, Y.-P. Sun, G. Chen, and S. Yan, Inducing and tuning Kondo screening in a narrow-electronic-band system, Nat. Commun. **13**, 2156 (2022).

[40] K. T. Law and P. A. Lee, 1T-TaS_2 as a quantum spin liquid, Proc. Natl. Acad. Sci. U.S.A. **114**, 6996 (2017).

[41] M. Klanjšek, A. Zorko, R. Žitko, J. Mravlje, Z. Jagličić, P. K. Biswas, P. Prelovšek, D. Mihailovic, and D. Arčon, A high-temperature quantum spin liquid with polaron spins, Nat. Phys. **13**, 1130 (2017).

[42] W.-Y. He, X. Y. Xu, G. Chen, K. T. Law, and P. A. Lee, Spinon Fermi Surface in a Cluster Mott Insulator Model on a Triangular Lattice and Possible Application to 1T-TaS_2, Phys. Rev. Lett. **121**, 046401 (2018).

[43] S. Mañas-Valero, B. M. Huddart, T. Lancaster, E. Coronado, and F. L. Pratt, Quantum phases and spin liquid properties of 1T-TaS_2, npj Quantum Mater. **6**, 69 (2021).

[44] D. Shin, N. Tancogne-Dejean, J. Zhang, M. S. Okyay, A. Rubio, and N. Park, Identification of the Mott Insulating Charge Density Wave State in 1T-TaS_2, Phys. Rev. Lett. **126**, 196406 (2021).

[45] Y. D. Wang, W. L. Yao, Z. M. Xin, T. T. Han, Z. G. Wang, L. Chen, C. Cai, Y. Li, and Y. Zhang, Band insulator to Mott insulator transition in 1T-TaS_2, Nat. Commun. **11**, 4215 (2020).

[46] W. Ruan, Y. Chen, S. Tang, J. Hwang, H.-Z. Tsai, R. L. Lee, M. Wu, H. Ryu, S. Kahn, F. Liou, C. Jia, A. Aikawa, C. Hwang, F. Wang, Y. Choi, S. G. Louie, P. A. Lee, Z.-X. Shen, S.-K. Mo, and M. F. Crommie, Evidence for quantum spin liquid behaviour in single-layer 1T-$TaSe_2$ from scanning tunnelling microscopy, Nat. Phys. **17**, 1154 (2021).

[47] F. Petocchi, C. W. Nicholson, B. Salzmann, D. Pasquier, O. V. Yazyev, C. Monney, and P. Werner, Mott versus Hybridization Gap in the Low-Temperature Phase of 1T-TaS_2, Phys. Rev. Lett. **129**, 016402 (2022).

[48] E. Tang, M. P. A. Fisher, and P. A. Lee, Low-energy behavior of spin-liquid electron spectral functions, Phys. Rev. B **87**, 045119 (2013).

[49] M. A. Altvater, S.-H. Hung, N. Tilak, C.-J. Won, G. Li, S.-W. Cheong, C.-H. Chung, H.-T. Jeng, and E. Y. Andrei, Revealing the charge density wave proximity effect in graphene on 1T-TaS_2, arXiv:2201.09195.

[50] V. Sunko, F. Mazzola, S. Kitamura, S. Khim, P. Kushwaha, O. J. Clark, M. D. Watson, I. Markovi, D. Biswas, L. Pourovskii, T. K. Kim, T.-L. Lee, P. K. Thakur, H. Rosner,

A. Georges, R. Moessner, T. Oka, A. P. Mackenzie, and P. D. C. King, Probing spin correlations using angle-resolved photoemission in a coupled metallic/Mott insulator system, Sci. Adv. **6**, eaaz0611 (2020).

[51] Y. Chen *et al.*, Strong correlations and orbital texture in single-layer 1*T*-TaS_2, Nat. Phys. **16**, 218 (2020).

[52] J. Rameau, H.-B. Yang, and P. Johnson, Application of the Lucy-Richardson deconvolution procedure to high resolution photoemission spectra, J. Electron Spectrosc. Relat. Phenom. **181**, 35 (2010).

[53] Y. He, Y. Wang, and Z.-X. Shen, Visualizing dispersive features in 2D image via minimum gradient method, Rev. Sci. Instrum. **88**, 073903 (2017).

[54] H. Katsura, N. Nagaosa, and P. A. Lee, Theory of the Thermal Hall Effect in Quantum Magnets, Phys. Rev. Lett. **104**, 066403 (2010).

[55] M. Z. Hasan and C. L. Kane, Colloquium: Topological insulators, Rev. Mod. Phys. **82**, 3045 (2010).

[56] X.-G. Wen, Topological orders and edge excitations in fractional quantum Hall states, Adv. Phys. **44**, 405 (1995).

[57] B. I. Halperin, Quantized Hall conductance, current-carrying edge states, and the existence of extended states in a two-dimensional disordered potential, Phys. Rev. B **25**, 2185 (1982).

[58] F. Wang, S. A. Kivelson, and D.-H. Lee, Nematicity and quantum paramagnetism in FeSe, Nat. Phys. **11**, 959 (2015).

[59] S. Lee, J.-G. Park, D. T. Adroja, D. Khomskii, S. Streltsov, K. A. McEwen, H. Sakai, K. Yoshimura, V. I. Anisimov, D. Mori, R. Kanno, and R. Ibberson, Spin gap in $Tl_2Ru_2O_7$ and the possible formation of Haldane chains in three-dimensional crystals, Nat. Mater. **5**, 471 (2006).